Theoretical study of lithium intercalation in rutile and anatase

Arvids Stashans,* Sten Lunell, and Robert Bergström
Department of Quantum Chemistry, Uppsala University, Box 518, S-751 20 Uppsala, Sweden

Anders Hagfeldt and Sten-Eric Lindquist
Department of Physical Chemistry, Uppsala University, Box 532, S-751 21 Uppsala, Sweden
(Received 16 June 1995)

Motivated by recent developments concerning coloration and energy storage in lithium intercalated nanostructural TiO_2, quantum chemical Hartree-Fock calculations have been carried out to study lithium atom intercalation in rutile and anatase. Equilibrium geometries and effective atomic charges were obtained for the rutile (110) and anatase (101) clean surfaces. Li-induced local one-electron energy levels were found in the gap between the upper valence band and the conduction band and could be attributed to Ti^{3+} states. The absorption energies obtained are compared with available experimental data. The equilibrium positions of the Li atom and its surrounding host atoms have been calculated for both structures. The results predict a higher possibility of lithium intercalation in the anatase structure than in rutile.

I. INTRODUCTION

Titanium dioxide is a fascinating material proving its usefulness in a wide range of applications. In catalytic and electrochemical applications, it has been utilized as a stable semiconductor electrode for the conversion of solar energy into chemical or electrical energy. Especially, the cleavage of water over TiO_2 using light energy is well known.[1] The degradation of organic pollutants present in wastewaters, using irradiated dispersions of TiO_2, is a fast growing field in basic and applied research.[2] One can also mention the use of TiO_2 in pigments, sun lotions, and toothpastes and its biocompatibility. The recent development of nanostructured TiO_2 electrodes[3] has also become the focus of many investigations.

The nanostructured TiO_2 films are of porous nature and are distinguished by a very high internal surface area. They are normally prepared by sol-gel procedures; the colloidal TiO_2 has anatase structure and the particles have a diameter of about 20 nm. Pores in the nanometer size range are constituted by the voids present between the semiconductor particles. The voids are interconnected and filled with an electrolyte. The roughness factor, defined as the ratio between the real and projected surface of the film, is, e.g., for a 10 μm thick film about 1000. The research and development of these systems are today expanding and one expects to find a variety of important applications.[4] Thus, dye-sensitized nanostructured TiO_2 electrodes have shown strikingly high photovoltaic conversion efficiencies.[5,6] Solar cell efficiencies up to 10%, at simulated solar intensity (AM 1.5, 96.4 mW/cm^2), have been obtained, showing good stability.[6]

Based on lithium intercalation these electrodes have been investigated for their use in batteries[7,8] and electrochromic devices.[9,10] Forward biasing of nanostructured TiO_2 films (anatase) in lithium-ion containing electrolytes, leads to electron accumulation in the TiO_2 lattice, charge compensated by Li^+ from the electrolyte. A charge capacity per unit weight of 265 mAh/g has been measured, which corresponds to a lithium insertion ratio of $x=0.8$ (Li_xTiO_2).[7] A rocking chair lithium battery with nanostructured TiO_2 (anatase) as the negative electrode and $LiCoO_2$ or $LiNi_{0.5}Co_{0.5}O_2$ as the positive electrode has been studied, showing energy densities over 100 mW/g and excellent performance over about 100 cycles (the experiments are still in progress).[8] Electron accumulation in TiO_2 also leads to a blue coloration, due to the creation of Ti^{3+} states (the extinction coefficient at 780 nm is 3400 L mol^{-1} cm^{-1}).[11] Because of the fact that nanostructured TiO_2 films (anatase) can be made completely transparent in the visible region, the electrochromic properties of these films are very interesting.[9,10] The investigation showed that Li intercalation led to rapid and reversible coloration. Absorption of $>90\%$ light throughout the visible and near IR could be switched on and off within a few seconds. It was also shown that the nanocrystalline morphology of the film played a primordial role in enhancing the electrochromic process.

Some of the fundamental questions which have arised during the investigations of Li intercalation in nanostructured TiO_2 electrodes concern the morphology of the electrode. Due to the high surface area of the TiO_2 film, one can expect a large degree of electron concentration in the TiO_2 material, where Li^+, situated in the electrolyte Helmholtz layer, charge compensates the electrons. In other words, one can expect a deep coloration from these systems simply due to surface effects, entering of Li^+ into the crystal lattice is actually not necessary. On the other hand, a Li-insertion ratio of 0.8 (see Ref. 7) does indicate Li intercalation in the anatase lattice. To what extent do we rely on surface effects in these systems and how efficient is the Li insertion into the TiO_2 structure? From the literature it is known that the uptake of Li^+ is much better in the anatase lattice compared to the rutile structure, in fact, rutile hardly inserts Li^+ at all.[12] The chemical nature of the Ti^{3+} state is also of great interest for a deeper understanding of Li intercalation in TiO_2. Experimentally, Ti^{3+} is said to be a localized energy level just below the conduction band edge consisting of Ti $3d$ orbitals (see Ref. 4 and references therein). Finally, the geometry of Li^+ ions in the TiO_2 crystal is of fundamental importance.

The objective of this paper is to approach the abovementioned questions by means of quantum chemical calculations. The position of Li^+ ions in both the rutile and the anatase structure is geometry optimized and the electronic and optical properties of these configurations will be presented. The surface effect is investigated by trying to put Li onto different surfaces. Here we have used the (110) surface and the (101) surface for the rutile and the anatase structure, respectively. From the literature the (110) surface appears to be the most stable one for rutile,[13] whereas the mostly exposed surface for nanostructured TiO_2 (anatase) films is (101).[14] Moreover, we also examine the possibility to exchange Ti ions by Li ions in the crystal structure and its consequences.

The paper is organized as follows. In Sec. II the computational details are described. In Sec. III the results of Li intercalation in TiO_2 structures and investigations of clean rutile (110) and anatase (101) surfaces are presented. The theoretical results are analyzed and compared with experimental data in Sec. IV. Section V, finally, contains conclusions and summary.

II. COMPUTATIONAL DETAILS

A. Modified INDO method

Nonempirical (*ab initio*) methods are still cumbersome and time consuming in the treatment of the electronic and spatial structure of complex systems, especially with partially covalent chemical bonding, like TiO_2 crystals. In this sense, the modified semiempirical intermediate neglect of differential overlap (INDO)[15] method as it is implemented in the CLUSTERD code[16] is very useful. It has been successfully employed to investigate a number of perfect and defective oxides[17–21] and materials with simpler structure. This technique is based on molecular orbital (MO) theory[22] and the periodic large unit-cell (LUC) method,[23] which calculates both the electronic structure and the total energy of the perfect crystal via MO as a linear combination of atomic orbitals. Usually an eightfold or even fourfold symmetric extension of the unit cell reproduces the distribution of the electronic density in the perfect crystal with sufficient accuracy. We used eight-times extended LUC with a total of 48 atoms ($Ti_{16}O_{32}$) and 96 atoms ($Ti_{32}O_{64}$) in the calculations of the perfect rutile, bulk and surface, and anatase bulk structures, respectively. A four-times extended LUC (48 atoms) was used in the calculations of the clean (perfect) anatase (101) surface.

The Fock matrix elements in the modified INDO approximation[15,16] contain a number of semiempirical parameters. The orbital exponent ζ enters the radial part of the Slater-type atomic orbitals:

$$R_{nl}(r)=(2\zeta)^{n+1/2}[(2n)!]^{-1/2}r^{n-1}\exp(-\zeta r), \quad (1)$$

where n is the principal quantum number of the valence shell. A valence basis set including $4s$, $4p$, $3d$ atomic orbitals (AO) on Ti and $2s$, $2p$ on the O atoms was used. The diagonal matrix elements of the interaction of an electron occupying the k'th valence AO on atom A with its own core are taken in the form

$$U^A_{kk}=-E^A_{\mathrm{neg}}(k)-\sum_m\left(P^{(0)A}_{mm}\gamma_{km}-\frac{1}{2}P^{(0)A}_{mm}K_{km}\right), \quad (2)$$

where $P^{(0)A}_{mm}$ are the diagonal elements of the density matrix ($=m$th AO populations), $E^A_{\mathrm{neg}}(k)$ is the kth AO electronegativity, γ_{km} and K_{km} are one-center Coulomb and exchange integrals, respectively. The matrix elements of an interaction of an electron on the k'th AO belonging to the atom A with the core of another atom B are calculated as

$$V_{kB}=Z_B\{1/R_{AB}+[\langle kk|mm\rangle-1/R_{AB}]\exp(-\alpha_{kB}R_{AB}\}, \quad (3)$$

where R_{AB} is the distance between atoms A and B, Z_B is the core charge of the atom B, α_{kB} is an adjustable parameter characterizing the nonpoint character of the atomic core B and additionally the diffuseness of the k'th AO, $\langle kk|mm\rangle$ is the two-center Coulomb integral. The last, so-called resonant integral parameter β_{AB}, enters the nondiagonal Fock matrix:

$$F^u_{km}=\beta_{AB}S_{km}-P^u_{km}\langle kk|mm\rangle, \quad (4)$$

where the k'th AO belongs to atom A and the mth AO to atom B, u is an electron subsystem with α or β spin, S_{km} is the overlap integral matrix between electrons on the kth and mth AO's, and P^u_{km} is the spin-density matrix.

Thus the parametrization scheme contains the following set of parameters: ζ, E_{neg}, $P^{(0)}$, α, and β. The INDO parameter set for the Ti atom was optimized by calculating the following data and comparing with experimental values: the main features of rutile and anatase crystals (width of the forbidden gap, widths of the O $2p$ and O $2s$ valence bands, the effective charges of the ions, and the structural parameters a,c,u for the bulk crystal) and the basic properties of Ti-containing molecules (equilibrium distance between the atoms in the molecule, the binding energy and the first ionization potential) (see Ref. 24). The details of the parametrization scheme of the modified INDO method are described in Ref. 16, where the standard parameter set for O atom is given as well. To find the nondiagonal α_{kB}, i.e., $\alpha_{\text{Ti-Li}}$ and $\alpha_{\text{Li-Ti}}$ parameters, the equilibrium distance between the atoms in the ^{4}TiLi molecule was fitted to the value, 2.91 Å, obtained from density-functional theory (DFT) calculations using the hybrid ''Becke3-LYP'' (Refs. 25 and 26) functional of the GAUSSIAN 92/DFT (Ref. 27) program, with a reasonably large basis set.[28] As a result these parameters have been calculated to be

$$\alpha_{\text{Ti-Li}}=0.1\ \text{a.u.}^{-1}, \quad (5)$$

$$\alpha_{\text{Li-Ti}}=0.32\ \text{a.u.}^{-1}. \quad (6)$$

Combining the LUC method with the INDO computational scheme described above we managed to explore the perfect TiO_2 crystals, bulk and surface. However, the periodic model has its limitations; the main one is the mutual perturbation of periodically arranged defects. That is why we chose the *embedded molecular cluster* (EMC) model[32] to study Li intercalation in the rutile and anatase crystals. The method is based on a strict treatment of the total energy of the whole crystal, accounting for the perturbation (polarization) that the remaining crystal has on the EMC region thereby leading to the so-called *quantum cluster* approach. The residual part of the crystal located beyond the EMC is

considered in the nonpoint charge approximation: the Coulomb interaction of the EMC electrons with atoms adjacent to the EMC boundary is considered in the same way as that for the atoms lying inside the EMC, although the AO's of the atoms adjacent to the EMC are constrained to have the same Löwdin populations[33] as those of the perfect lattice, i.e., using the density matrix of the perfect crystal obtained in a separate LUC calculation and taking into account explicitly the AO's of the outside atoms. The contribution of the infinite number of the latter atoms is calculated exactly by means of the Ewald method.[34] The matrix elements of the total Coulomb field produced by the non-point-charge outer region is added to the diagonal elements of the Fock matrix of the EMC, although the angular dependence of the AO's in the Coulomb integrals is neglected. Thus, the Coulomb part of the interaction of the cluster atoms with the atoms in the remaining crystal is taken into account, while within the cluster all interactions between atoms are included at the INDO-level approximation. The difference in the interaction between cluster atoms and those between cluster and the nonpoint embedding ions, results in a relaxed cluster configuration in which the boundary atoms are slightly displaced inwards (4–5 % and 2–4 % of the interatomic distances for the rutile and anatase, respectively) from their positions in the perfect lattice. Because of the ionic-covalent bonding in the titanium dioxide, the clusters were constructed following the idea of localized groups of electrons or *structural elements* (SE).[32] The crux of this procedure is to construct a cluster having an integer number of SE's (TiO_2 molecular units, in our case) which allows one to consider more correctly the interaction between such a cluster and the remaining crystal due to smaller correlation effects between the SE's mentioned above (for more details see Ref. 32).

B. Calculation of the hole trapping energy

It is known (see review articles, Refs. 35 and 36) that $[M]^0$ and $[M]^+$ impurity centers (M=Li, Na) can cause hole trapping in II-VI compounds by simply changing their charge state. Something similar is found theoretically in TiO_2, the rutile polymorph, when a Li ion substitutes Ti in the regular lattice site (see below). Since Li^+ is differently charged than the Ti atoms in the perfect TiO_2 lattice, its presence strongly perturbs the occupied $2p$ states of the surrounding O ions. This results in the formation of resonant states within the valence band and rapid hole self-trapping in the lattice. To calculate the energy gain due to this process,

$$\Delta E_{\mathrm{TH}} = E_{\mathrm{TH}} - E_F^{(k)}, \tag{7}$$

where E_{TH} is the hole energy for the fully relaxed trapped hole (TH) state, while $E_F^{(k)}$ is the energy of the free-hole state, we used the method described in Refs. 37 and 38. This method realizes the idea of Gilbert and Stoneham[39,40] who considered hole self-trapping as a hypothetical two-stage procedure: localization of a free hole in a local perfect crystal region in the first stage, and the subsequent relaxation of the lattice with accompanying electronic redistribution in a local region during the second stage. The hole acquires a positive energy due to the loss of kinetic energy in the local state in the first stage. In the second stage the hole acquires a negative energy due to (i) the crystal relaxation around the defective region, (ii) the gain in the energy caused by the formation of chemical bonds in the local region, and (iii) the polarization energy associated with the rest of the EMC lattice outside the local region. Therefore the energy gain can be calculated as a difference:

$$\Delta E_{\mathrm{TH}} = E_{\mathrm{loc}} + E_{\mathrm{rel}}, \tag{8}$$

where $E_{\mathrm{loc}}>0$ but $E_{\mathrm{rel}}<0$. The relaxation energy, E_{rel}, was calculated using the EMC method with a quantum cluster $[LiTi_{15}O_{32}]^+$. To calculate the localization energy, E_{loc}, we used the quantum cluster $[Ti_{16}O_{32}]^+$ and an eight-times extended LUC, i.e., in the latter case we calculated the localization energy of a hypothetical *self-trapped* hole occurring in a *pure* rutile lattice (for more details see Ref. 37).

III. RESULTS

A. Clean rutile (110) surface

The exploration of the clean rutile (110) surface was performed using the periodic LUC, 2×2×2, i.e., eight-times extended unit cell, method. This is equivalent to a band-structure calculation at eight **k** points in the Brillouin zone. The surface features were calculated with a single-slab model, consisting of six atomic layers, 48 atoms in total, which was finite in the ⟨110⟩ direction and had two-dimensional (2D) periodicity in the ⟨001⟩ and ⟨110⟩ directions. The bulk lattice constants, a=4.418 Å, c=3.014 Å, u=0.307, were fitted before;[24] the corresponding experimental[41] values are a=4.594 Å, c=2.959 Å, u=0.305. We assumed that the surface is nonmagnetic and therefore the restricted Hartree-Fock method was used in all clean surface calculations.

A relaxation of the atomic layers was performed which showed the following pattern: two atomic layers consisting of bridging oxygens, situated on both sides of the slab, relaxed inward by 0.12 Å, the two next surface layers relaxed inward by 0.03 Å, whereas no displacements of the atoms of the two middle layers were observed. The optimized atomic geometry configuration was then used for the electronic-structure calculations.

A consistent picture for the effective charges of the ions was observed: the charges reach their maximal value, Q(Ti) =+2.45 **e** and Q(O)=−1.23 **e**, in the middle of the slab. These values are close to the bulk charges, Q(Ti)=+2.52 **e** and Q(O)=−1.26 **e**, found in our previous investigation[24] using a LUC with 3D periodicity. The effective charges reduce in the direction ⟨110⟩ until they reach the value of Q(O) =−0.91 **e** for the bridging oxygens. Note that the charge difference for the *unrelaxed* slab was even larger, i.e., Q(O) =−1.24 **e** for the O atoms placed in the middle slab and Q(O)=−0.78 **e** for the bridging O atoms. Due to surface effects the one-electron bandgap, i.e., the gap between the upper valence band and the conduction band, decreased from the calculated bulk value of ΔE_g^b=7.4 eV to ΔE_g^s=5.9 eV. The values of the calculated optical bandgaps by the self-consistent field (ΔSCF) method (i.e., as the differences of total energies of the LUC before and after the excitation of an electron from the highest occupied MO to the lowest unoccupied MO) differ in the same manner: ΔE_g^b=5.7 eV and ΔE_g^s=5.0 eV.

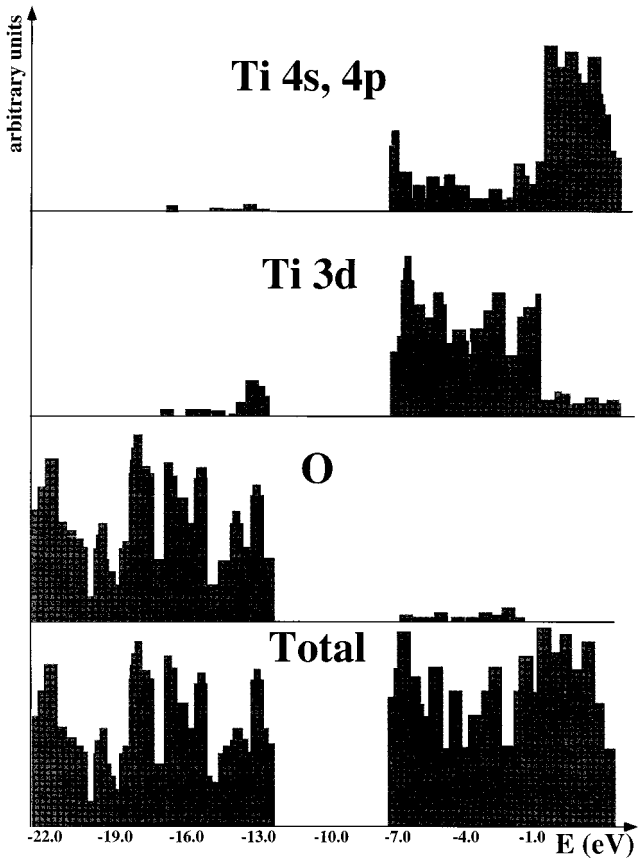

FIG. 1. Density of states (DOS) for the upper valence band and the conduction band of the rutile (110) surface. Note that the bandgap, obtained directly from the one-electron energies, is overestimated in this figure, and also in Figs. 2–4 (see text).

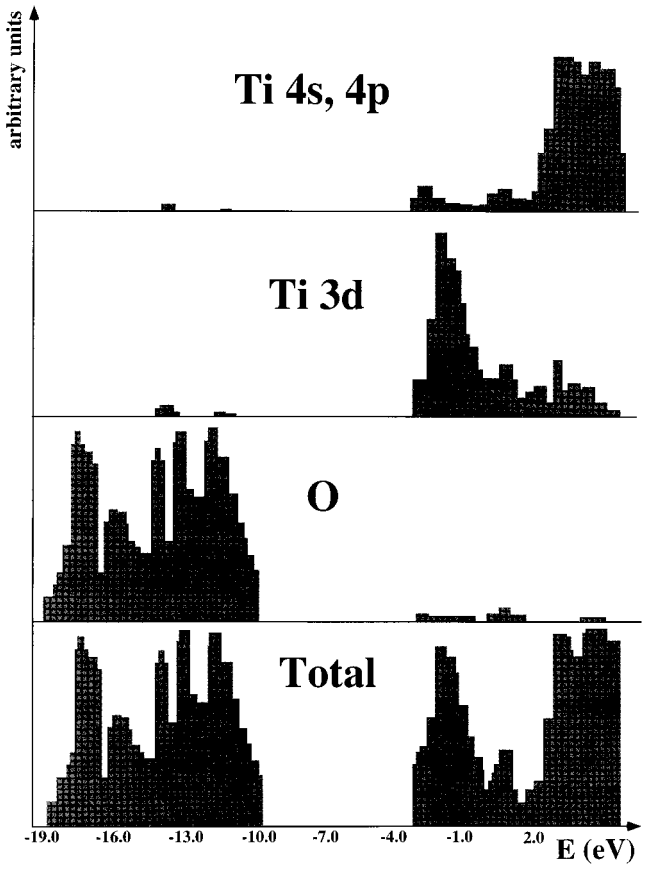

FIG. 2. DOS for the upper valence band and the conduction band of the rutile bulk.

The density of states (DOS) for Ti $4s$, $4p$, Ti $3d$, O $2p$, and the total DOS are plotted in comparison with the corresponding bulk patterns in Figs. 1 and 2, respectively. The upper valence band is composed mainly of O $2p$ states, although at the top there is a considerable contribution of Ti $3d$ and a smaller amount of Ti $4s$. This suggests a rather covalent character of the chemical bonding in the rutile structure. The degree of the admixture of Ti states in the upper valence band is higher for the (110) surface band in comparison to the bulk band structure. The conduction band is in both cases composed mainly of Ti $4s$, Ti $3d$ (lower part) and Ti $4p$ states (upper part).

B. Clean anatase (101) surface

The exploration of a clean anatase (101) surface was done using $2\times1\times2$, i.e., four-times extended LUC with a total of 48 atoms. This was simulated as a single-slab, consisting of nine atomic layers and having 2D periodicity in the $\langle 101\rangle$ and $\langle 010\rangle$ directions and being finite in the $\langle 101\rangle$ direction. The bulk constants, $a=3.641$ Å, $c=9.197$ Å, $u=0.203$, fitted previously[24] were used. The corresponding experimental[41] values are $a=3.784$ Å, $c=9.515$ Å, $u=0.208$.

Relaxation of the atomic layers was performed which showed an inward displacements of the outer layers from both sides of the slab by 0.05 Å, the next-outer layers by 0.03 Å, and next two layers by less as 0.02 Å. No displacements were observed of the atoms situated in the central atomic layers. Similarly to the rutile (110) surface described above, the optimized geometry was used later for the electronic structure calculations.

The effective charges calculated for this model did not differ so much depending on their position in the slab. The maximal effective charges were observed in the center of the slab, $Q(\mathrm{Ti})=+2.35$ **e** and $Q(\mathrm{O})=-1.22$ **e**, the minimal effective charges were found on atoms situated on the slab's periphery, $Q(\mathrm{Ti})=+2.26$ **e** and $Q(\mathrm{O})=-1.04$ **e**. The calculated effective charges of the ions in the anatase bulk, LUC with 3D periodicity were found to be $Q(\mathrm{Ti})=+2.30$ **e** and $Q(\mathrm{O})=-1.15$ **e**. The one-electron bandgap in Figs. 3 and 4 is only a little larger for the bulk band structure, $\Delta E_g^b=7.5$ eV, than in the case of the (101) surface, for which we obtained $\Delta E_g^s=7.2$ eV. The values of the calculated optical bandgaps by the ΔSCF method are $\Delta E_g^b=5.8$ eV and $\Delta E_g^s=5.5$ eV for the four-times extended LUC with 3D and 2D periodicity, respectively. The DOS pattern for the anatase (101) surface is described in Fig. 3, while the anatase bulk band structure is shown in Fig. 4. The most significant distinction from the similar rutile DOS patterns is that in the case of anatase, Ti $4p$ states were found only in the upper part of the conduction band, while in the rutile case they are spread over the whole conduction band.

C. Li intercalation in the rutile bulk and surface

A 49-atom quantum stoichiometric cluster $[LiTi_{16}O_{32}]^0$, consisting of 16 molecular units TiO_2, with an added Li

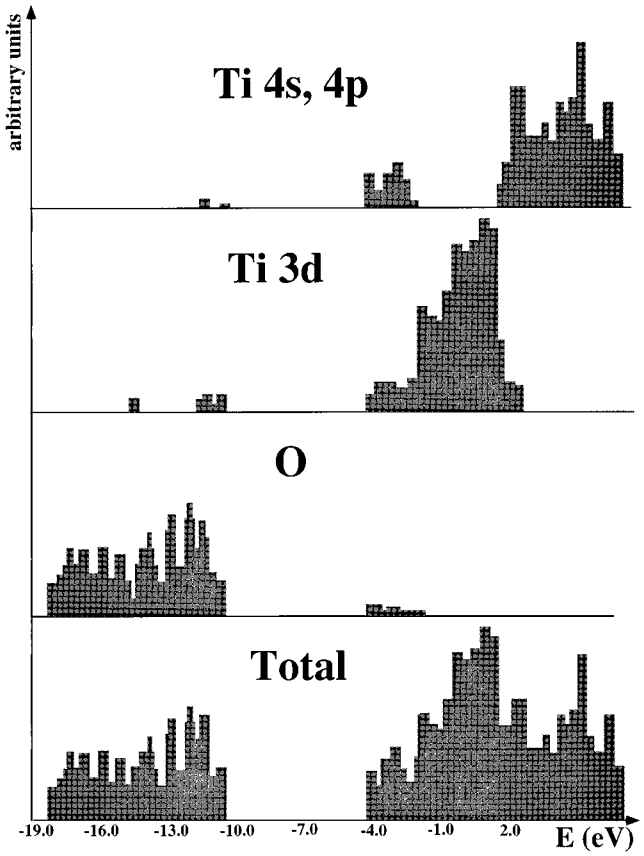

FIG. 3. DOS for the upper valence band and the conduction band of the anatase (101) surface.

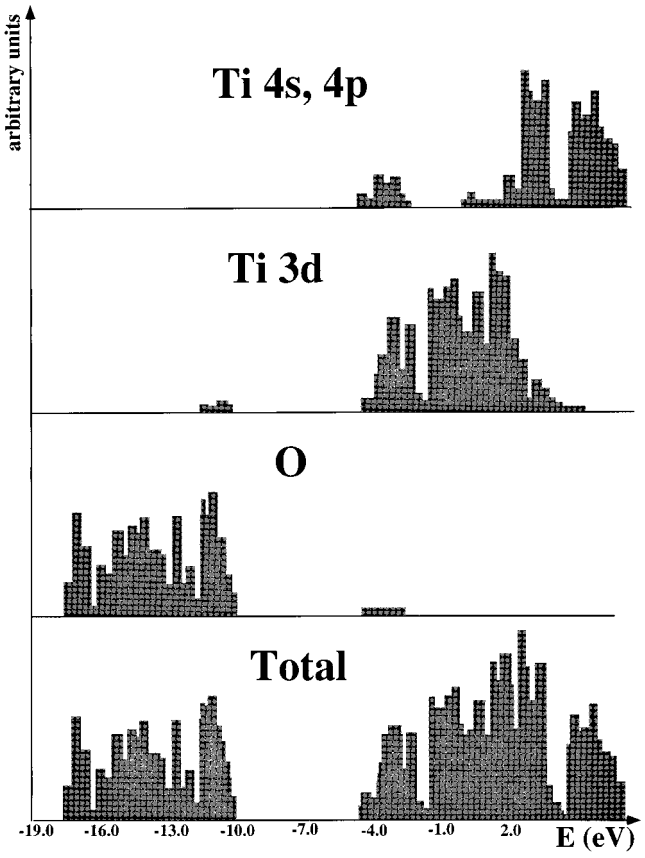

FIG. 4. DOS for the upper valence band and the conduction band of the anatase bulk.

atom, was taken for the Li intercalation simulations in bulk rutile. After geometry optimization of the perfect $[Ti_{16}O_{32}]^0$ cluster and lithium insertion, the Li atom was allowed to relax, assuming no *a priori* pattern of its possible interstitial position. The automated relaxation was carried out using the facilities of the CLUSTERD code. During the relaxation two equilibrium interstitial positions of Li atom were obtained, marked further as *case A* and *case B*.

For case *A*, the equilibrium position of the inserted lithium is shown in Fig. 6. It is situated on the line connecting the two titanium atoms, Ti(1) and Ti(2), 1.49 Å from the Ti(1) and 1.46 Å from the Ti(2). After the Li found its minimal energy state, the ten nearest atoms were allowed to relax. The outcome of the displacements is shown in Table I. As one can see, due to the positive effective charge of the Li atom, the surrounding titanium ions move outwards while the negatively charged oxygen ions move towards the Li impurity. Li is expected to lose its valence electron which transfers to the closest Ti(2) ion, see Table II. As a result the local one-electron energy level in the gap between the upper valence band and the conduction band is composed mainly of Ti(2) 4*s* AO's. This level, marked *a* in Fig. 5, is situated 1.6 eV above the top of the upper valence band, with respect to the perfect rutile bands, and is responsible for the absorption transitions given in Table IV. The latter were found as the difference of the total energies for the self-consistent ground and excited states (ΔSCF method). Note that the unoccupied states *b* (composed mainly of Ti $4p_x$ and Ti $4p_y$ AO's) and *c* (composed mainly of Ti $4p_z$ AO's) are situated in the conduction band whereas after population by an excited electron they fall into the gap between the upper valence band and the conduction band.

TABLE I. Displacements of atoms surrounding the Li impurity in $[LiTi_{16}O_{32}]^0$ cluster (rutile structure) (in Å). A "−" sign denotes displacements of the atoms towards Li while a "+" sign denotes displacements in the opposite direction.

Atom	Case A[a]	Case B[b]
Ti(1)	+0.18	+0.06
Ti(2)	+0.14	+0.06
Ti(3)		+0.02
Ti(4)	+0.02	+0.35
Ti(5)	+0.10	
O(1)	−0.18	0.14[c]
O(2)	−0.16	0.14[c]
O(3)	−0.05	
O(4)	−0.06	
O(5)	−0.02	−0.39
O(6)	+0.03	−0.02

[a]The ten atoms closest to Li were allowed to relax.

[b]The eight atoms closest to Li were allowed to relax.

[c]Atoms O(1) and O(2) in case *B* move as shown in Fig. 6, angle $\beta=12°$.

TABLE II. The effective charges of the atoms in the perfect $[Ti_{16}O_{32}]^0$ and imperfect $[LiTi_{16}O_{32}]^0$ clusters (rutile structure) (in e).

	Perfect cryst.	Case *A*	Case *B*
Li		0.72	0.83
Ti(1)	2.39	2.21	2.37
Ti(2)	2.39	1.50	2.39
Ti(3)	2.39	2.36	2.39
Ti(4)	2.21	2.21	1.15
Ti(5)	2.21	2.24	2.22
O(1)	−1.14	−1.08	−1.04
O(2)	−1.13	−1.13	−1.11
O(3)	−1.12	−1.12	−1.13
O(4)	−1.12	−1.10	−1.12
O(5)	−1.13	−1.13	−1.06
O(6)	−1.13	−1.02	−1.14

In case *B*, the Li atom finds itself placed 1.76 Å from Ti(4), 1.95 Å from Ti(1), 1.58 Å from O(2), 1.60 Å from O(1) and 2.65 Å from O(5) (see Fig. 6; the angle α is equal to 42°). After relaxation of the eight atoms in the vicinity of the defect the nearest titanium ions were found to move outwards, especially Ti(4) which receives an electron (see Tables I and II), while oxygens, on the contrary, move towards the interstitial Li atom, which is obviously due to the Coulomb electrostatic interaction. The direction of displacements of O(1) and O(2) is apparently caused by two effects: (i) the considerable outward displacement of Ti(4) which leaves an extra space for these two oxygens and (ii) the quite close initial placing of the O(1) and O(2) atoms to the Li impurity, not allowing this distance to reduce more. The chemical nature of the local level *a*, situated 0.9 eV above the top of the upper valence band, as well as the virtual

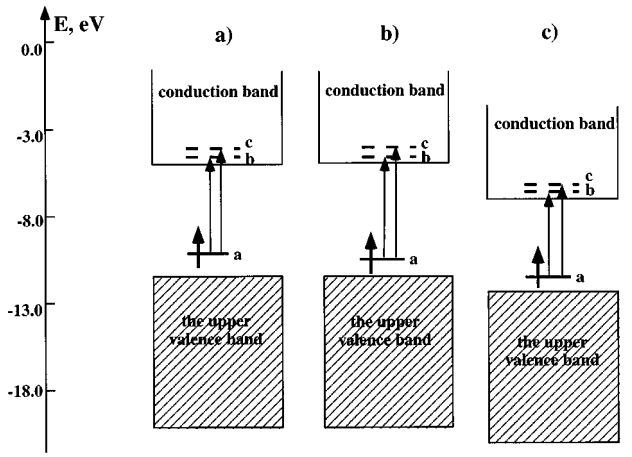

FIG. 5. Calculated positions of the Li-induced local levels within the rutile bandgap for the cases when Li is situated in position *A* (a) and *B* (b) of the rutile bulk and when it finds the equilibrium position on the rutile (110) surface (c). Level *a* denotes the ground state and levels *b* and *c* unoccupied excited states. The arrows show the possible transitions. The position of the local level *a* is 1.6 eV (a), 0.9 eV (b), and 0.7 eV (c), respectively, above the top of the upper valence band of the pure crystal.

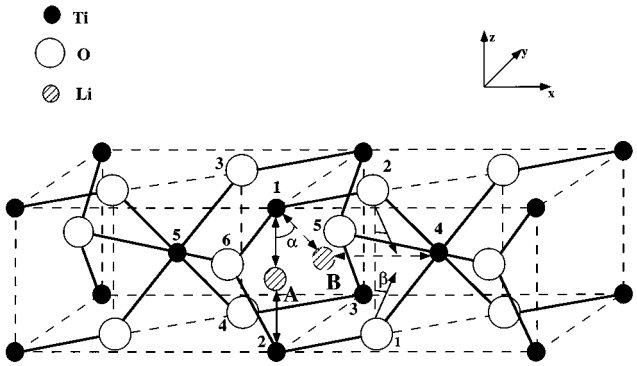

FIG. 6. The two equilibrium positions of the inserted Li atom in the rutile bulk: (i) case *A* when lithium finds the minimal energy position on the line connecting Ti(1) and Ti(2) atoms, and (ii) case *B* when it is situated 1.76 Å from the Ti(4). The arrows show the direction of the displacements of the O(1) and O(2) atoms.

levels *b* and *c* are similar to those in case *A*. The calculated absorption energies are described in Table IV. In case *B* the total energy of the system is lower which implies that this could be an energetically more favorable position than the case *A*. The distance between the two Li-interstitial equilibrium positions is 1.31 Å. For rutile, problems with the self-consistent convergency were encountered, and large displacements of the surrounding defect atoms were found. These effects are due to the difficulties of Li intercalation in the rutile structure, i.e., Li can be intercalated with larger probability in the anatase structure than in rutile (see Secs. III D and IV for more details).

The calculation of Li intercalation in the rutile (110) surface was carried out using a molecular cluster in the form of

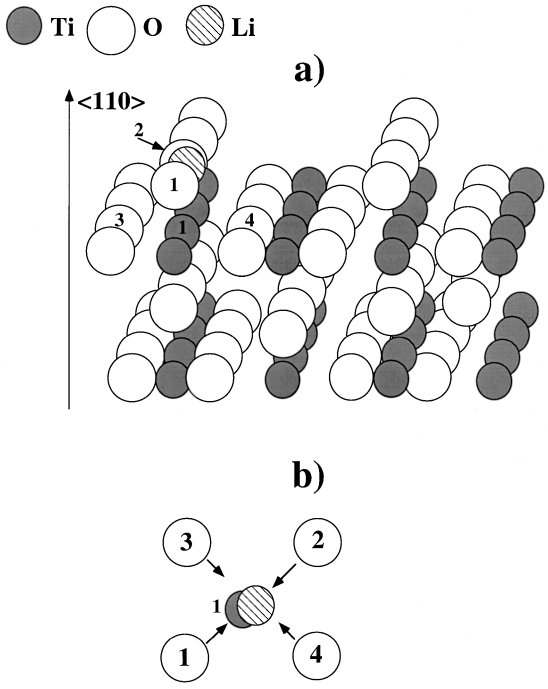

FIG. 7. The equilibrium position between two bridging oxygens for a Li atom intercalated on the rutile (110) surface (a) and the directions of displacements of Li-surrounding atoms on the surface (b).

TABLE III. The effective charges of the atoms in the clean and Li-intercalated rutile surfaces (in e).

Atom	Q (perf. surface)	Q (def. surface)
Li		0.94
Ti(1)	2.18	1.37
O(1)	−0.91	−1.00
O(2)	−0.91	−1.02
O(3)	−1.20	−1.18
O(4)	−1.20	−1.21

the eightfold extended (2×2×2) LUC of the rutile described above. It was observed that the equilibrium position of the Li atom is right on the surface between two bridging oxygen atoms (see Fig. 7) almost above the titanium atom Ti(1). Similar to the bulk calculations the nearest atoms on the surface were allowed to relax, which resulted in shifts of the two bridging oxygens, O(1) and O(2), by 0.25 Å each and 0.06 Å displacements of the two oxygens, O(3) and O(4), towards the Li atom. The closest Ti(1) atom moved away by 0.07 Å. The local level a found in the energy gap is situated 0.7 eV above the top of the upper valence band and is composed of 4s AO's of Ti(1), which receives an electron (see Table III), with a strong admixture of Ti $3d_{x^2-y^2}$ AO's. The chemical nature of the corresponding virtual states, b and c, is similar to those in the bulk band structure. The calculated absorption energies are shown in Table IV.

D. Li intercalation in the anatase bulk and surface

A 97-atom stoichiometric EMC $[LiTi_{32}O_{64}]^0$ consisting of 32 molecular units, TiO_2, with an added Li atom was used for the lithium intercalation study in the anatase bulk. Finally, the minimal energy position for the Li atom in the anatase structure was found to be in one of the structural voids (see Fig. 8): it is situated 2.25 Å from Ti(1), 2.81 Å from O(1), 1.86 Å from O(2), and 1.81 Å from O(5). After this procedure, the Li-neighboring atoms were allowed to relax. As one can see from Table V, the closest Ti atoms move outwards while the surrounding O atoms move towards the Li atom. These shifts are smaller in magnitude than the corresponding movements of atoms in the rutile lattice (see Table I for comparison). An electron from the lithium is transferred to the nearest, Ti(1), atom (see Table V). As a result the local one-electron energy level a, situated 1.8 eV (see Fig. 9) above the top of the upper valence band, is composed mainly of Ti 4s AO's of Ti(1). The chemical nature of the three corresponding virtual levels are as follows: the b state is composed of Ti $4p_x$ with a considerable admixture of Ti $4p_y$ AO's; the c state is composed of Ti $4p_y$ with a considerable admixture of Ti $4p_z$ AO's; the d state is composed mainly of Ti $4p_z$ AO's. The calculated absorption energies are shown in Table VI.

TABLE IV. Calculated absorption energies (in eV) with a Li atom intercalated in the rutile structure.

Transition	Case A	Case B	(110) surface
$a \rightarrow b$	0.9	0.5	1.6
$a \rightarrow c$	1.0	0.6	1.9

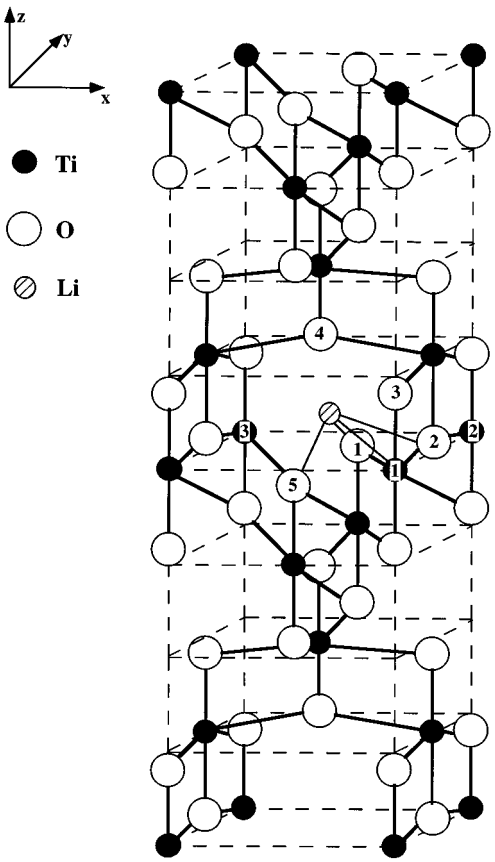

FIG. 8. The equilibrium position of the inserted Li atom in the anatase bulk, in one of the anatase structural voids.

The calculation of Li intercalation in the anatase (101) surface was performed using a molecular cluster in the form of the fourfold extended (2×1×2) LUC of the anatase lattice described in Sec. III B. The equilibrium position of the Li atom was found to be in one of the anatase structural interstitial positions (see Fig. 10). After the lithium found its minimal energy position, the four nearest O atoms and the

TABLE V. Displacements of atoms surrounding the Li impurity in a $[LiTi_{32}O_{64}]^0$ cluster (anatase structure) (in Å) and the effective charges of the corresponding atoms in the perfect and Li-intercalated clusters. A "−" sign denotes displacements of the atoms towards the Li ion, while a "+" sign denotes displacements in the opposite direction.

Atom	ΔR	Q (perf. cluster)	Q (def. cluster)
Li			0.79
Ti(1)	+0.12	2.24	1.62
Ti(2)	+0.03	2.26	2.16
Ti(3)	+0.03	2.26	2.17
O(1)	−0.05	−1.03	−1.05
O(2)	−0.09	−1.17	−1.28
O(3)	−0.04	−1.17	−1.16
O(4)	−0.06	−1.03	−1.06
O(5)	−0.03	−1.04	−1.05

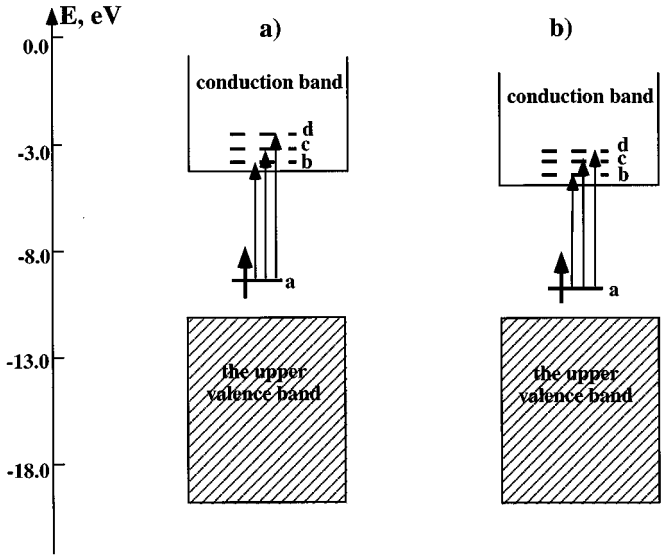

FIG. 9. Calculated positions of the Li-induced local levels within the bandgap for the cases when Li is intercalated in the bulk (a) and in the (101) surface (b) of the anatase structure. Level *a* denotes the ground state and levels *b*, *c*, and *d* unoccupied excited states. The arrows show the possible transitions. The position of the local level *a* is 1.8 eV (a) and 0.9 eV (b), respectively, above the top of the upper valence band of the pure crystal.

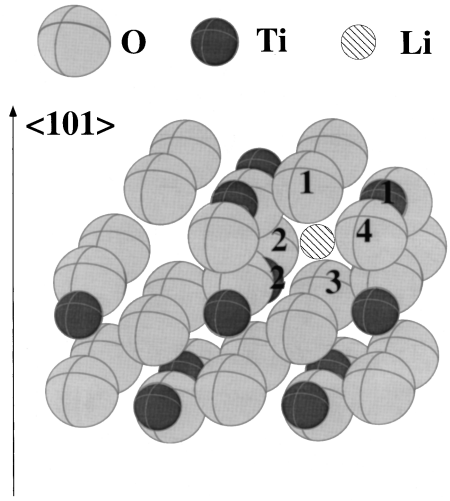

FIG. 10. Li intercalation into the anatase (101) surface. The minimal energy position is shown and the Li-surrounding atoms which are allowed to relax are marked.

two nearest Ti atoms were allowed to relax. As a result, O(1) and O(4) moved 0.06 Å while O(2) and O(3) moved 0.04 Å towards the Li atom. The two nearest titaniums, Ti(1) and Ti(2), shifted outwards by 0.03 and 0.10 Å, respectively. The local one-electron energy level found in the bandgap is situated 0.9 eV above the top of the upper valence band and is composed mainly of $4s$ and $3d_{x^2-y^2}$ AO's of Ti(2) which receives an electron (see Table VII). The chemical nature of the corresponding virtual levels—*b*, *c*, and *d*—is as follows: *b* is composed of Ti $4p_y$ AO's, *c* is composed of Ti $4p_x$ AO's with an admixture of Ti $4p_z$ AO's of the same Ti(2), and finally *d* is composed of Ti $4p_z$ AO's with an admixture of the $3d$ AO's of the same Ti(2) and $4p$ AO's of the nearest Ti atoms. The calculated absorption energies are given in Table VI.

E. Trapped hole near a Li impurity in the rutile crystal

The defects responsible for the coloration of materials are often due to paramagnetic hole centers, most of which absorb light in the visible and near-visible region. The Li ion substituting a Ti ion in the regular lattice site of the rutile crystal, has an effective charge $\leqslant 1.0$ **e**, i.e., it has a considerably lower charge than the Ti ion in the perfect lattice of the rutile crystal [$q(\mathrm{Ti}) = +2.4$ **e**]. This is the reason why Li ions can trap positively charged holes occurring in the rutile due to, e.g., ionizing radiation.

We have simulated a Li-induced trapped hole (TH) using a $[\mathrm{LiTi_{15}O_{32}}]^+$ EMC with the Li ion substituting the central Ti ion (see Fig. 11). After geometry optimization of the defective region, it was found that the hole can be shared by two O atoms situated near the Li impurity leading to a *two-site* hole model [see Fig. 11(a)] or it can be localized on a *single* O atom when it moves towards lithium (see Fig. 11(b)].

During the formation of the two-site TH, O(1) and O(2) move towards each other reducing the O(1)-O(2) distance from the initial value of 2.39 to 1.95 Å. The direction of displacement is described by an angle $\alpha = 17°$ [see Fig. 11(a)]. The hole trapping is accompanied by the creation of a chemical bond between O(1) and O(2). The bond populations were calculated as follows:

$$q_{AB} = \sum_{\mu \in A} \sum_{\nu \in B} S_{\mu\nu} P_{\mu\nu} \tag{9}$$

where $P_{\mu\nu}$ are elements of the bond-order matrix and $S_{\mu\nu}$ are overlap integrals for the AO's μ and ν of the atoms *A* and *B*, respectively. The obtained O(1)-O(2) bond population is 0.16 **e**, while in the perfect rutile crystal the bond populations

TABLE VI. Calculated absorption energies (in eV) with a Li atom intercalated in the anatase structure.

Transition	Bulk	(101) surface
$a \rightarrow b$	1.7	1.3
$a \rightarrow c$	2.0	1.8
$a \rightarrow d$	2.5	1.9

TABLE VII. The effective charges of the atoms in the perfect and Li-intercalated anatase surfaces (in *e*).

Atom	*Q* (perf. surface)	*Q* (def. surface)
Li		0.86
Ti(1)	2.27	2.23
Ti(2)	2.35	1.66
O(1)	−1.04	−1.06
O(2)	−1.13	−1.14
O(3)	−1.15	−1.15
O(4)	−1.04	−1.07

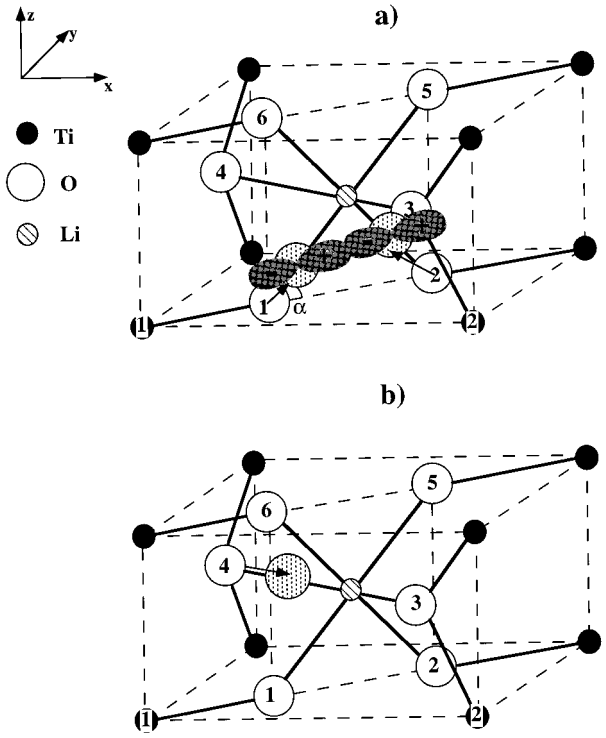

FIG. 11. Models of a two-site trapped hole described by an antibonding σ_u orbital (a) and a one-site trapped hole (b) near the Li impurity in the rutile structure.

between oxygen atoms were equal to 0.0 **e**. Note, that this rather large value, 0.16 **e**, is comparable to the bond populations between Ti and O atoms in the perfect rutile structure, $q_{\text{Ti-O}}=0.17$ **e** (apical bond) and $q_{\text{Ti-O}}=0.28$ **e** (equatorial bond). The relaxation energy reduces the total energy of the system by 5.2 eV and as a result the calculated TH energy (see Table VIII) is 3.9 eV without the inertial polarization energy associated with the rest of the lattice outside the TH region. The two-site hole is shared mainly by two O atoms, about 70% of the hole charge is found on them (see Table IX). It occupies an antibonding σ-type MO along the $\langle 110\rangle$ axis [see Fig. 11(a)], where σ_u is a one-electron wave function consisting of the $2p_x$ and $2p_y$ AO's of the two O atoms constituting the TH; its energy level lies within the conduction band.

The modeling of the one-site Li-induced hole was carried out within the same EMC. It was found that during the formation of the TH in the direction $\langle 100\rangle$, the oxygen, which

TABLE VIII. Different contributions to the trapped hole energy (in eV) for the two-site and one-site holes.

	Two-site hole	One-site hole
E_{rel}	5.2	3.9
E_{loc}[a]	1.3	1.2
ΔE_{TH}[b]	3.9	2.7

[a]Obtained using the method described in Ref. 15.

[b]Without the inertial polarization energy around the trapped hole region.

TABLE IX. The analysis of Li-trapped hole charge density distribution (in e) on atoms in the defective region.

	Perfect crystal	Two-site hole	One-site hole
Li		0.89	0.89
O(1)	−1.14	−0.79	−1.07
O(2)	−1.15	−0.82	−1.08
O(3)	−1.13	−1.06	−1.07
O(4)	−1.13	−1.06	−0.55
O(5)	−1.14	−1.12	−1.11
O(6)	−1.16	−1.14	−1.08
Ti(1)	2.39	2.35	2.36
Ti(2)	2.39	2.33	2.37

receives the hole, moves towards the Li atom by 0.38 Å, reducing the O-Li distance to 1.19 Å. The calculated relaxation energy E_{rel} is equal to 3.9 eV. Finally, the TH energy is 2.7 eV which is less than in the case of the two-site hole. Therefore, one can conclude that the two-site hole trapped by a Li impurity is energetically more favorable than the one-site TH.

Our interest in TH simulations was concerned with their contribution to the absorption spectra of the rutile crystal with inserted Li. Therefore, a calculation of the absorption energy for the most energetically favorable, two-site TH, was carried out using the ΔSCF method (see Fig. 12). The excited state π_u is described by a one-electron wave function consisting of the $2p_z$ AO's of the two O atoms constituting the TH; its level lies within the conduction band. The value obtained for the absorption energy is 1.2 eV.

IV. DISCUSSION

The main purpose of the calculations was to model Li atom intercalation in rutile and anatase, both for bulk crystals

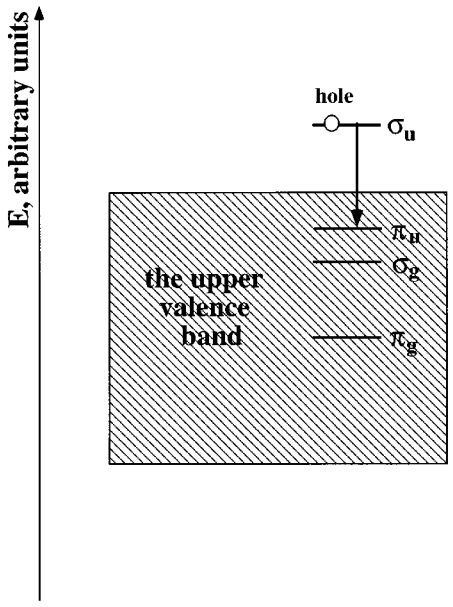

FIG. 12. The absorption transition for a two-site trapped hole occurring in the rutile crystal due to a Li ion substituting a Ti ion.

and for the above described surfaces. Still, the exploration of the clean rutile (110) and anatase (101) surfaces is of fundamental importance.

The rutile (110) surface was adopted as a model for our theoretical investigation because of its stability and because of the large amount of experimental data reported recently.[42,43] The obtained results show rather large displacements of the bridging oxygens of the outer layers (Fig. 7) while the relaxation of the atoms placed in the central layers is small and is similar to the previous *ab initio* computations.[44] This suggests that the rutile (110) surface is stable and does not require a considerable rearrangement or reconstruction.[45,46] The creation of the surface leads to the appearance of O $2p$ states in the conduction band and especially Ti $3d$ states in the upper-valence-band region (of Figs. 1 and 2). No occupied O $2p$ states occur in the bandgap, in accordance with the experimental observations.[47,48] The calculated surface bandgap, 5.0 eV, is substantially overestimated compared to the experimental value[42] of 1.6 eV. The error originates from the Hartree-Fock one-determinant approximation[22] which does not take into account correlation corrections, consisting of short-range and long-range components. Only short-range corrections, which, in fact, have atomic character, are effectively taken into account in the course of our parameter fitting. The long-range corrections cannot be taken into account through atomic parameters since they occur due to crystal polarization by an electron and hole, obviously having many-center nature. The long-range corrections are not calculated for TiO_2 crystals; estimates for other oxides give values of 3–4 eV.[18,49,50] Despite this shortcoming, we have reproduced correctly the decreasing nature of the bandgap value due to the surface effects. The calculated effective charges, using Löwdin population analysis,[33] point out the strong covalent effects in the chemical bonding of the rutile crystal and agree very well with *ab initio* calculations.[44]

The anatase (101) surface is stable and the mostly exposed one[14,51,52] but has so far lacked theoretical investigation. In the present paper, we report a theoretical study of the band-structure features and geometrical properties using the periodic LUC method. The qualitative conclusions which can be drawn from our calculations suggest that the anatase (101) surface has a larger ionic contribution to the chemical bonding than the rutile (110) surface. This follows from the rather high effective charges of the atoms, situated even in the outer layers of the slab. The surface bandgap value, 5.5 eV, is comparable to the corresponding bulk quantity, 5.8 eV. The diminutive relaxation of the atomic layers along the $\langle 101 \rangle$ direction implies the stability of the surface under study and agrees with the experimental expectations.[14]

The bottom of the conduction band (Figs. 1–4) is predominantly Ti $3d$ in character with some Ti $4s$, $4p$ content, which differs slightly from the previous investigations of TiO_2 band structure[53–55] arguing for a pure Ti $3d$ conduction band.

The results of Li atom intercalation presented in the Sec. III argue for the preference of the anatase structure for such a process. This is because of structural voids, where the lithium could be placed without a big distortion of the perfect crystal lattice. Since the rutile has a more compact arrangement of the host atoms, the insertion of a Li impurity leads to a reduction of lattice stability and as a result one can expect rather large displacements of the Li surrounding atoms. This showed up as trouble in the self-consistent convergency of the calculations in both cases, *A* and *B*, of the lithium intercalation study in the rutile bulk. The preference of Li intercalation in anatase follows also from a few known experimental studies.[12,56,57]

The exploration of the optical properties of Li-intercalated TiO_2 crystals points to the following mechanism of a charge transfer; after the Li atom is inserted, the electron occupying the Li $2s$ AO moves to the closest Ti atom; as a result, a local state in the bandgap occurs. This Li-induced local state can be described by a MO consisting mainly of Ti $4s$ AO or Ti $4s$ with an admixture of Ti $3d$ AO's, in the case of bulk and surface studies, respectively. After the excitation of an electron to the corresponding excited (virtual) one-electron level, the latter finds itself situated below the bottom of the conduction band. Note that the ΔSCF energies should be discussed rather than the difference of the relevant one-electron (orbital) energies, which give only rough estimates for the absorption energies in the case of local energy levels. The calculated broad absorption spectra, 1.7–2.5 eV and 1.3–1.9 eV for the anatase bulk and (101) surface, respectively, correspond very well with the experimentally observed coloration of nanoporous TiO_2 (anatase) films after lithium intercalation.[9,10] The absorption energies for the rutile (110) surface, 1.6 and 1.9 eV, also fall into the same region of absorption spectra and can be compared to the experimental data reported in Ref. 58. One can note that these excitations are local in nature and therefore not expected to be subject to the long-range correlation errors which effect the calculated bandgaps discussed before.

In the case when a Li ion substitutes the Ti ion in the regular lattice site of the rutile structure, a hypothetical trapped hole occurrence is expected. If such an object is stable, which needs additional experimental evidence, then it contributes to the absorption spectra of Li-intercalated TiO_2. The absorption energy, 1.2 eV, falls into the experimentally observed[58] wide absorption spectra region.

V. CONCLUSIONS

We have presented a theoretical study of lithium intercalation in the rutile and anatase structures of TiO_2. The calculations indicate that Li intercalation is easier in the anatase structure than in rutile. This can be related to the much larger distortions of the bulk lattice occurring upon Li intercalation in rutile compared to anatase, where structural voids can accommodate the Li atoms. Moreover, in the case of the rutile (110) surface, the lithium intercalation seems to be mainly a surface effect since the Li atom does not penetrate into the bulk. The calculated absorption energies, due to the lithium insertion, form a wide absorption spectrum: 1.7–2.5 eV and 1.3–1.9 eV for the anatase bulk and the (101) surface, respectively, and 1.6–1.9 eV for the rutile (110) surface which agrees with the experimentally measured spectra.[9,10]

ACKNOWLEDGMENTS

The authors would like to express their thanks to Robin W. Grimes and Eugene Stefanovich for helpful and stimulating discussions. This work was supported by the Swedish Research Council for Engineering Sciences (TFR) and the commission of the European Community Joule II programme.

*On leave from Institute of Solid State Physics, University of Latvia, 8 Kengaraga Str., LV-1063 Riga, Latvia.

[1] A. Fujishima and K. Honda, Nature (London) **238**, 37 (1972).
[2] O. Legrini, E. Oliveros, and A. M. Braun, Chem. Rev. **93**, 671 (1993).
[3] B. O'Regan, J. Moser, M. Anderson, and M. Grätzel, J. Phys. Chem. **94**, 8720 (1990).
[4] A. Hagfeldt and M. Grätzel, Chem. Rev. **95**, 49 (1995).
[5] B. O'Regan and M. Grätzel, Nature (London) **353**, 737 (1991).
[6] M. K. Nazeruddin, A. Kay, I. Rodicio, R. Humphry-Baker, E. Müller, P. Liska, N. Vlachopoulos, and M. Grätzel, J. Am. Chem. Soc. **115**, 6382 (1993).
[7] S. Huang, L. Kavan, A. Kay, and M. Grätzel, Act. Pass. Elec. Comp. **18**, 23 (1995).
[8] S. Huang, L. Kavan, I. Exnar, and M. Grätzel, J. Electrochem. Soc. **142**, 142 (1995).
[9] A. Hagfeldt, N. Vlachopoulos, and M. Grätzel. J. Electrochem. Soc. **141**, L82 (1994).
[10] A. Hagfeldt, N. Vlachopoulos, S. Gilbert, and M. Grätzel, Proc. SPIE **2255**, 297 (1994).
[11] G. Rothenberger, D. Fitzmaurice, and M. Grätzel, J. Phys. Chem. **96**, 5983 (1992).
[12] B. Zachau-Christiansen, K. West, T. Jacobsen, and S. Atlung, Solid State Ionics **28**, 1176 (1988).
[13] V. E. Henrich, Rep. Prog. Phys. **48**, 1481 (1985).
[14] M. Grätzel (private communication).
[15] A. Shluger, Theor. Chim. Acta **66**, 355 (1985).
[16] E. V. Stefanovich, E. K. Shidlovskaya, A. L. Shluger, and M. A. Zakharov, Phys. Status Solidi B **160**, 529 (1990).
[17] A. L. Shluger and N. Itoh, J. Phys. Condens. Matter **2**, 4119 (1990).
[18] P. W. M. Jacobs, E. A. Kotomin, A. Stashans, E. V. Stefanovich, and I. Tale, J. Phys. Condens. Matter **4**, 7531 (1992).
[19] E. V. Stefanovich, A. L. Shluger, and C. R. A. Catlow, Phys. Rev. B **49**, 11 560 (1994).
[20] A. Stashans, E. A. Kotomin, and J.-L. Calais, Phys. Rev. B **49**, 14 854 (1994).
[21] E. A. Kotomin, A. Stashans, L. N. Kantorovich, A. I. Livshicz, A. I. Tale, and J.-L. Calais, Phys. Rev. B **51**, 8770 (1995).
[22] J. Pople and D. Beveridge, *Approximate MO Theories* (McGraw-Hill, New York, 1970).
[23] A. L. Shluger and E. V. Stefanovich, Phys. Rev. B **42**, 9664 (1990).
[24] A. Stashans, S. Lunell, and R. W. Grimes (unpublished).
[25] A. D. Becke, J. Chem. Phys. **98**, 5648 (1993).
[26] C. Lee, W. Yang, and R. G. Parr, Phys. Rev. B **37**, 785 (1988).
[27] M. J. Frisch, G. W. Trucks, H. B. Schlegel, P. M. W. Gill, B. G. Johnson, M. W. Wong, J. B. Foresman, M. A. Robb, M. Head-Gordon, E. S. Replogle, R. Gomperts, J. L. Andres, K. Raghavachari, J. S. Binkley, C. Gonzalez, R. L. Martin, D. J. Fox, D. J. DeFrees, J. Baker, J. J. P. Stewart, and J. A. Pople, GAUSSIAN 92/DFT Revision G.3, Gaussian Inc., Pittsburgh, PA, 1993.
[28] In the DFT calculations a (nonrelativistic) effective core potential (Ref. 29) was used for Ti. The basis set for the $3s$, $3p$, $3d$, and $4s$ electrons was derived from the minimal basis in Ref. 29; a (5/5/5)/[3311/2111/311] contraction was used with an additional diffuse p function (exponent 0.0053) added. For Li a triple zeta valence quality (Ref. 30) basis set with two p polarization functions (exponents 0.40 and 0.06) was used. Earlier calculations on titanium containing molecules with the Becke3-LYP functional and similar quality basis sets have given quite accurate equilibrium geometries (Ref. 31), the ^{4}TiLi molecule is, however, quite weakly bound ($E_{\mathrm{dis}}\approx 0.61$ eV with Becke3-LYP), which means that the uncertainty in the bond length could still be rather large.
[29] P. J. Hay and W. R. Wadt, J. Chem. Phys. **82**, 299 (1985).
[30] A. Schäfer, C. Huber, and R. Ahlrichs, J. Chem. Phys. **100**, 5829 (1994).
[31] R. Bergström, L. A. Eriksson, and S. Lunell, Int. J. Quantum Chem. (to be published).
[32] L. N. Kantorovich, J. Phys. C **29**, 5041 (1988).
[33] P.-O. Löwdin, J. Chem. Phys. **18**, 365 (1950).
[34] M. Born and K. Huang, *Dynamic Theory of Crystal Lattices* (Oxford University Press, London, 1954).
[35] A. L. Shluger and A. M. Stoneham, J. Phys. Condens. Matter **5**, 3049 (1993).
[36] Y. Chen and M. M. Abraham, J. Phys. Chem. Solids **51**, 747 (1990).
[37] L. Kantorovich, A. Stashans, E. Kotomin, and P. W. M. Jacobs, Int. J. Quantum Chem. **52**, 1177 (1994).
[38] L. Kantorovich, E. Heifets, A. Livshicz, M. Kuklja, and P. Zapol, Phys. Rev. B **47**, 14 875 (1993).
[39] T. L. Gilbert (unpublished).
[40] A. M. Stoneham, *Theory of Defects in Solids* (Oxford University Press, London, 1975).
[41] S. C. Abrahams and J. L. Bernstein, J. Chem. Phys. **55**, 3206 (1971). M. Horn, C. F. Schwerdtfleger, and E. P. Meagher, Z. Kristallogr. **136**, 273 (1972).
[42] K. Sakamaki, K. Itoh, A. Fujishima, and Y. Gohshi, J. Vac. Sci. Technol. A **8**, 614 (1990).
[43] J.-M. Pan, B. L. Maschhoff, U. Diebold, and T. E. Madey, J. Vac. Sci. Technol. A **10**, 2470 (1992).
[44] P. Reinhardt and B. A. Hess, Phys. Rev. B **50**, 12 015 (1994).
[45] B. L. Maschoff, J.-M. Pan, and T. E. Madey, Surf. Sci. **259**, 190 (1991).
[46] A. E. Taverner, P. C. Hollamby, P. S. Aldridge, and R. G. Egdell, Surf. Sci. **287/288**, 653 (1993).
[47] V. E. Henrich, G. Dresselhaus, and H. F. Zeiger, Phys. Rev. Lett. **36**, 1355 (1976).
[48] R. H. Tait and R. V. Kasowski, Phys. Rev. B **20**, 5178 (1979).
[49] W. B. Fowler, Phys. Rev. **151**, 657 (1966).
[50] A. B. Kunz, Phys. Rev. B **6**, 606 (1972).
[51] D. G. Wiesler, M. F. Toney, M. G. Samant, O. R. Melroy, C. S. McMillan, and W. H. Smyrl, Surf. Sci. **268**, 57 (1992).
[52] C. Ludwig and P. W. Schindler, J. Colloid. Interface Sci. **169**, 284 (1995).
[53] S. Munnich and M. Schmeits, Phys. Rev. B **28**, 7342 (1983).
[54] S. Munnich and M. Schmeits, Phys. Rev. B **31**, 3369 (1985).

[55] M. Tsukada, C. Satoko, and H. Adachi, J. Phys. Soc. Jpn. **47**, 1610 (1979).
[56] B. Zachau-Christiansen, K. West, T. Jacobsen, and S. Skaarup, Solid State Ionics **53/56**, 364 (1992).
[57] M. P. Cantão, J. I. Cisneros, and R. M. Torresi, J. Phys. Chem. **98**, 4865 (1994).
[58] C.-G. Granqvist, *Handbook of Inorganic Electrochromic Materials* (Elsevier, Amsterdam, 1995).